


## Spectral Functions of the Holstein Polaron: Exact and Approximate Solutions

Petar Mitrić<sup>1</sup>, Veljko Janković<sup>1</sup>, Nenad Vukmirović<sup>1</sup>, and Darko Tanasković<sup>1</sup>  
*Institute of Physics Belgrade, University of Belgrade, Pregrevica 118, 11080 Belgrade, Serbia*

 (Received 10 January 2022; revised 2 May 2022; accepted 5 August 2022; published 22 August 2022)

It is generally accepted that the dynamical mean field theory gives a good solution of the Holstein model, but only in dimensions greater than two. Here, we show that this theory, which becomes exact in the weak coupling and in the atomic limit, provides an excellent, numerically cheap, approximate solution for the spectral function of the Holstein model in the whole range of parameters, even in one dimension. To establish this, we make a detailed comparison with the spectral functions that we obtain using the newly developed momentum-space numerically exact hierarchical equations of motion method, which yields electronic correlation functions directly in real time. We crosscheck these conclusions with our path integral quantum Monte Carlo and exact diagonalization results, as well as with the available numerically exact results from the literature.

DOI: [10.1103/PhysRevLett.129.096401](https://doi.org/10.1103/PhysRevLett.129.096401)

The Holstein model is the simplest model that describes an electron that propagates through the crystal and interacts with localized optical phonons [1]. On the example of this model, numerous many-body methods were developed and tested [2]. The Holstein molecular crystal model is also very important in order to understand the role of polarons (quasiparticles formed by an electron dressed by lattice vibrations) in real materials [3]. This is still a very active field of research fueled by new directions in theoretical studies [4–12] and advances in experimental techniques [13].

The Holstein model can be solved analytically only in the limits of weak and strong electron-phonon coupling [14–16]. Reliable numerical results for the ground state energy and quasiparticle effective mass were obtained in the late 1990s using the density matrix renormalization group (DMRG) [17,18] and path integral quantum Monte Carlo (QMC) methods [19], and also within variational approaches [20–22]. At the time, numerically exact spectral functions for one-dimensional (1D) systems were obtained only within the DMRG method [17,18]. The main drawback of the QMC method is that it gives correlation functions in imaginary time and obtaining spectral functions and dynamical response functions is often impossible since the analytical continuation to the real frequency is a numerically ill-defined procedure. Interestingly, at finite temperature the spectral functions were obtained only very recently using finite- $T$  Lanczos (FTLM) [23] and finite- $T$  DMRG [24] methods. All these methods have their strengths and weaknesses depending on the parameter regime and temperature. As usually happens in a strongly interacting many-body problem, a complete physical picture emerges only by taking into account the solutions obtained with different methods.

The hierarchical equations of motion (HEOM) method is a numerically exact technique that has recently gained

popularity in the chemical physics community [25–28]. It has been used to explore the dynamics of an electron (or exciton) linearly coupled to a Gaussian bosonic bath. Within HEOM, we calculate the correlation functions directly on the real time (real frequency) axis [29]. Nevertheless, the applications of the HEOM method to the Holstein model [30–34] have been, so far, scarce because of the numerical instabilities stemming from the discreteness of the phonon bath on a finite lattice.

Along with numerically exact methods, a number of approximate techniques have been developed and applied to the Holstein model [35–38]. The dynamical mean field theory (DMFT) is a simple nonperturbative technique that has emerged as a method of choice for the studies of the Mott physics within the Hubbard model [39,40]. It can also be applied to the Holstein model giving numerically cheap results directly on the real frequency axis [41]. This method fully takes into account local quantum fluctuations and it becomes exact in the limit of infinite coordination number when the correlations become completely local. It was soon recognized [42,43] that the DMFT gives qualitatively correct spectral functions and conductivity for the Holstein model in three dimensions. In low-dimensional systems the solution is approximate as it neglects the nonlocal correlations and one might expect that the DMFT solution would not be accurate, particularly in one dimension. Surprisingly, to our knowledge, only the DMFT solution for the Bethe lattice was used in comparisons with the numerically exact results for the ground state properties in one dimension [20,44]. The quantitative agreement was rather poor, suggesting that the DMFT cannot provide a realistic description of the low-dimensional Holstein model due to the importance of nonlocal correlations [16,20,44].

In this Letter, we present a comprehensive solution of the 1D Holstein model: (i) We solve the DMFT equations in all

parameter regimes. At zero temperature we find a remarkable agreement of the DMFT ground state energy and effective mass with the available results from the literature in one, two, and three dimensions. (ii) For intermediate electron-phonon coupling, we obtain numerically exact spectral functions using the recently developed momentum-space HEOM approach [45]. For strong coupling we calculate the spectral functions using exact diagonalization (ED). We find a very good agreement with DMFT results and therefore demonstrate that the DMFT is rather accurate, in sharp contrast to current belief in the literature. (iii) We crosscheck the results with our QMC calculations in imaginary time. Overall, we demonstrate that the DMFT emerges as a unique method that gives close to exact spectral functions in the whole parameter space of the Holstein model, both at zero and at finite temperature.

*Model and methods.*—We study the 1D Holstein model given by the Hamiltonian

$$H = -t_0 \sum_i (c_i^\dagger c_{i+1} + \text{H.c.}) - g \sum_i n_i (a_i^\dagger + a_i) + \omega_0 \sum_i a_i^\dagger a_i. \quad (1)$$

Here,  $c_i^\dagger$  ( $a_i^\dagger$ ) are the electron (phonon) creation operators,  $t_0$  is the hopping parameter, and  $n_i = c_i^\dagger c_i$ . We consider dispersionless optical phonons of frequency  $\omega_0$ , and  $g$  denotes the electron-phonon coupling parameter.  $t_0$ ,  $\hbar$ ,  $k_B$ , and lattice constant are set to 1. We consider the dynamics of a single electron in the band. It is common to define several dimensionless parameters: adiabatic parameter  $\gamma = \omega_0/2t_0$ , electron-phonon coupling  $\lambda = g^2/2t_0\omega_0$ , and  $\alpha = g/\omega_0$ . These parameters correspond to different physical regimes of the Holstein model shown schematically in Fig. 1(a).

In order to obtain reliable solutions in the whole parameter space, we use two approximate methods and three methods that are numerically exact. In the Holstein model, the DMFT reduces to solving the polaron impurity problem in the conduction electron band supplemented by the self-consistency condition [41]. The impurity problem can be solved in terms of the continued fraction expansion, giving the local Green's function on the real frequency axis (see Ref. [41] and Supplemental Material (SM) [46], Sec. I, for details). A crucial advantage of the DMFT for the Holstein model is that it becomes exact in both the weak coupling and in the atomic limit, and that it can be easily applied in the whole parameter space both at zero and at finite temperature. The DMFT equations can be solved on a personal computer in just a few seconds to a few minutes depending on the parameters. On general grounds, the DMFT is expected to work particularly well at high temperatures when the correlations become more local due to the thermal fluctuations [47,48]. We will compare the DMFT with the well-known self-consistent Migdal

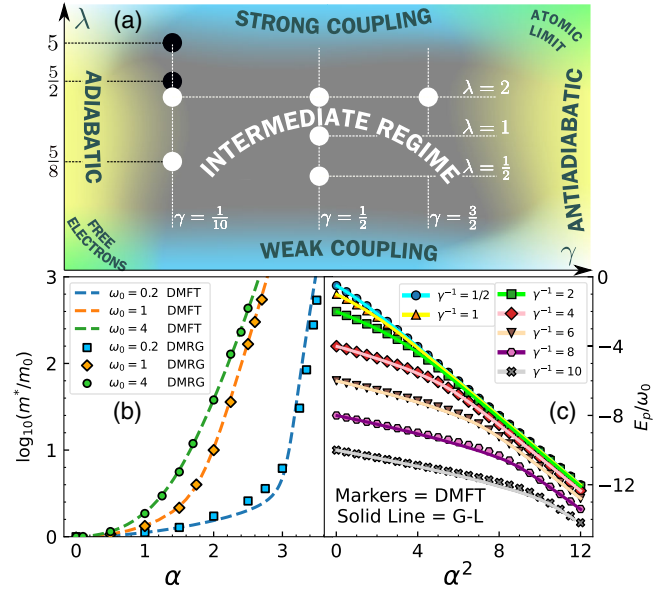


FIG. 1. (a) Schematic plot of different regimes in the  $(\gamma, \lambda)$  parameter space. The white (black) circles correspond to parameters for which both HEOM and QMC (just QMC) calculations were performed. The DMFT results are obtained in practically whole space of parameters. (b) Comparison of the DMFT and DMRG (taken from Refs. [17,20]) renormalized electron mass at  $T = 0$ . (c) Comparison of the ground state energy from the DMFT and the global-local variational approach (taken from Ref. [20]) at  $T = 0$ .

approximation (SCMA) [49], which becomes exact only in the weak coupling limit; see Sec. II of SM [46].

We have recently developed the momentum-space HEOM method [45] that overcomes the numerical instabilities originating from the discrete bosonic bath. Within this method we calculate the time-dependent greater Green's function  $G^>(k, t)$ , which presents the root of the hierarchy of the auxiliary Green's functions. The hierarchy is, in principle, infinite, and one actually solves the model by truncating the hierarchy at certain depth  $D$ . The HEOM are propagated independently for each allowed value of  $k$  up to long times ( $\omega_0 t_{\max} \sim 500$ ). The propagation takes 5 to 10 hours on 16 cores per momentum  $k$ . The discrete Fourier transform is then used to obtain spectral functions without introducing any artificial broadening. Numerical error in the HEOM solution can originate from the finite-size effects since the method is applied on the lattice with  $N$  sites, and also from the finite depth  $D$ . We always use  $N$  and  $D$ , as given in SM [46], which correctly represent the thermodynamic limit. Generally, for larger  $g$  we need smaller  $N$  and larger  $D$ . This is why the ED method with a small number of sites could be a better option in the strong coupling regime. The ED method can be used more efficiently after the initial Hamiltonian is transformed by applying the Lang-Firsov transformation; see SM [46], Sec. III.

In the QMC method, we calculate the correlation function  $C_k(\tau) = \langle c_k(\tau) c_k^\dagger \rangle_{T,0}$  in imaginary time. The thermal

expectation value is performed over the states with zero electrons and  $c_k(\tau) = e^{\tau H} c_k e^{-\tau H}$ . We use the path integral representation, the discretization of imaginary time, and analytical calculation of integrals over the phonon coordinates. We then evaluate a multidimensional sum over the electronic coordinates by a Monte Carlo method. This method is a natural extension of early works where such approach was applied just to thermodynamic quantities [50–52]. Details of the method are presented in Ref. [45].

*Results at zero temperature.*—In Fig. 1(b), we show the DMFT results for the electron effective mass at the bottom of the band,  $m^*/m_0 = 1 - d\text{Re}\Sigma(\omega)/d\omega|_{E_p}$  (where  $\Sigma(\omega)$  is the self-energy), over a broad range of parameters covering practically the whole parameter space in the  $(\gamma, \lambda)$  plane. We see that the mass renormalization is in striking agreement with the DMRG result [17,20] that presents the best available result from the literature. Small discrepancies are visible only for stronger interaction with small  $\omega_0$ . A similar level of agreement can be seen in the comparison of the ground state (polaron) energy  $E_p$  in Fig. 1(c). Here, the results obtained with variational global-local method [20,21] are taken as a reference. While the agreement in the weak coupling and in the atomic limit could be anticipated since the DMFT becomes exact in these limits, we find the quantitative agreement in the crossover regime between these two limits rather surprising, having in mind that the DMFT completely neglects nonlocal correlations. It is also interesting that this was not observed earlier. The only difference from the standard reference of Ciuchi *et al.* [41] is that we applied the DMFT to the 1D case, as opposed to the Bethe lattice. This is, however, a key difference. Otherwise the DMFT provides only a qualitative description of the Holstein model [3,16,20,44,53]. From the technical side, the only difference as compared to the case of the Bethe lattice is in the self-consistency equation. For obtaining a numerically stable and precise solution, it was crucial to use an analytical expression for the self-consistency relation (see Sec. IB in SM [46]). We have also calculated the effective mass for two- and three-dimensional lattices (see Sec. IC in SM [46]) and the agreement with the QMC calculation from Ref. [19] is excellent. This was now expected since the importance of nonlocal correlations decreases in higher dimensions. A comparison with the Bethe lattice effective mass is illustrated in SM [46], Sec. ID.

The next step is to check if the agreement with the numerically exact solution extends also to spectral functions. Typical results at  $k = 0$  are illustrated in Fig. 2. We note that at  $T = 0$  the DMFT quasiparticle peak is a delta function (broadened in Fig. 2), while satellite peaks are incoherent having intrinsic nonzero width. In HEOM, the peak broadening due to the finite lattice size  $N$  and finite propagation time  $t_{\text{max}}$  is generally much smaller than the Lorentzian broadening used in the insets of Figs. 2(a)–2(d). The weights of the DMFT and HEOM quasiparticle peaks

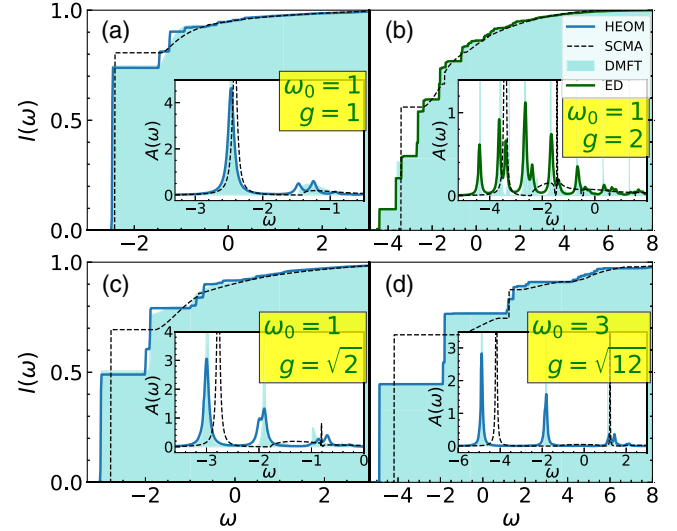


FIG. 2. (a)–(d) Integrated HEOM, DMFT, SCMA, and ED spectral weight,  $I(\omega) = \int_{-\infty}^{\omega} d\nu A_k(\nu)$ , for  $k = 0$  and  $T = 0$ . The insets show comparisons of the spectral functions.  $I(\omega)$  is obtained without broadening, whereas  $A(\omega)$  is broadened by Lorentzians of half-width  $\eta = 0.05$ .

correspond to the  $m_0/m^*$  ratio. The satellite peaks are also very well captured by the DMFT solution in all parameter regimes. For  $g = 1$  we can see two small peaks in the first satellite structure of the HEOM solution. We find very similar peaks also in the DMFT solution when applied on a lattice of the same size, which is here equal to 10 (see SM [46], Sec. IV). Hence, we conclude that these peaks are an artefact of the finite lattice size. In the strong coupling regime  $\omega_0 = 1, g = 2$ , the DMFT is compared with ED since the thermodynamic limit is practically reached for  $N = 4$ ; see SM [46], Sec. IV. Here, we notice a pronounced excited quasiparticle peak [22,23] whose energy is below  $E_p + \omega_0$ . This peak, which consists of a polaron and a bound phonon, is also very well resolved within the DMFT solution. For parameters in Fig. 2(d) the lattice sites are nearly decoupled, approaching the atomic limit ( $t_0 \ll g, \omega_0$ ), when the DMFT becomes exact (see Sec. V in SM [46]). For a comparison, we show also the SCMA spectral functions. As the interaction increases, the SCMA solution misses the position and the weight of the quasiparticle peak and the satellite peaks are not properly resolved. Further comparisons of zero temperature spectral functions are shown in Sec. VI of SM [46].

*Results at finite temperature.*—Reliable finite- $T$  results for the spectral functions of the Holstein model have been obtained only very recently using the FTLM [23] and finite- $T$  DMRG methods [24]. Here, we calculate the spectral functions using HEOM or ED and compare them extensively with the DMFT. The results are crosschecked using the QMC results in imaginary time.

Typical results for the spectral functions are shown in Fig. 3, while additional results for other momenta and other

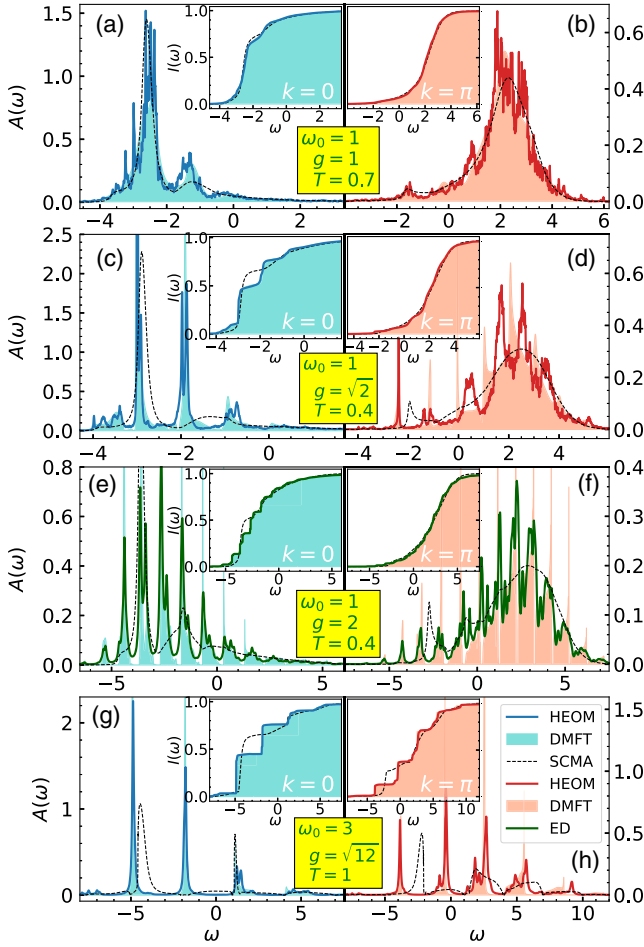


FIG. 3. (a)–(h) Spectral functions at  $T > 0$  for  $k = 0$  and  $k = \pi$ . In panels (e)–(f) only the ED results are broadened by Lorentzians of half-width  $\eta = 0.05$ , while all the curves are broadened in (g)–(h) with the same  $\eta$ . All insets are shown without broadening.

parameters are shown in Sec. VII of SM [46]. We see that for  $T > 0$  the satellite peaks appear also below the quasiparticle peak. The agreement between the DMFT and the HEOM (ED) spectral functions is very good. The agreement remains excellent even for  $g = 2$  where the electrons are strongly renormalized  $m^*/m_0 \approx 10$ , which is far away from both the atomic and weak coupling limits, where the DMFT is exact. A part of the difference between the DMFT and the HEOM (ED) results can be ascribed to the small finite-size effects in the HEOM and ED solutions, as detailed in SM [46], Sec. IV. In accordance with the presented results, it is not surprising that the self-energies are nearly  $k$  independent, as shown in SM [46], Sec. VIII. It is also instructive to examine the difference between the SCMA and DMFT (HEOM) solutions. For moderate interaction [Figs. 3(a) and 3(b)], the weight of the SCMA quasiparticle peak is nearly equal to the DMFT (HEOM) quasiparticle weight, and the overall agreement of spectral functions is rather good. This is not the case for stronger

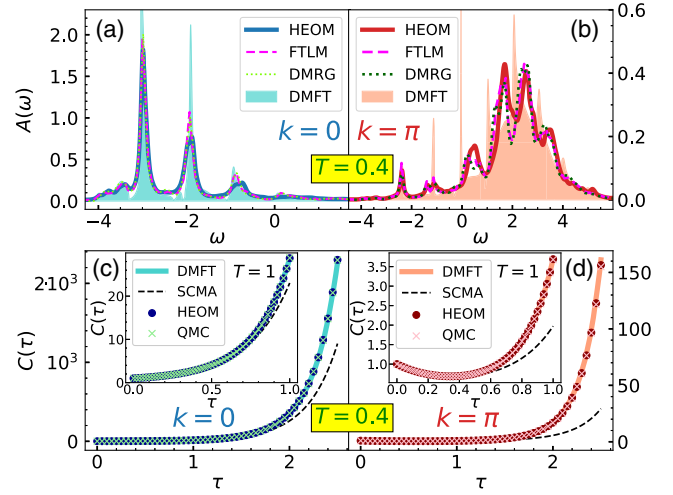


FIG. 4. (a), (b) Comparison of DMFT, HEOM, and finite- $T$  DMRG and FTLM (taken from Ref. [24]) spectral functions at  $T = 0.4$ . All the lines are here broadened by Lorentzians of half-width  $\eta = 0.05$ . (c), (d) DMFT, QMC, HEOM, and SCMA imaginary time correlation functions at  $T = 0.4$  ( $T = 1$  in the insets). Here,  $g = \sqrt{2}$ ,  $\omega_0 = 1$ .

electron-phonon coupling [Figs. 3(c)–3(h)] where the SCMA poorly approximates the true spectrum.

We observe that for  $g = \sqrt{2}$  and  $k = \pi$  the DMFT and HEOM satellite peaks are somewhat shifted with respect to one another; see Figs. 3(c) and 3(d). This is the most challenging regime for the DMFT, representing a crossover ( $\lambda = 1$ ) between the small and large polaron. Nevertheless, the agreement remains very good near the quasiparticle peak for  $k = 0$ , which will be the most important for transport in weakly doped systems. In order to gain further confidence into the details of the HEOM spectral functions for  $g = \sqrt{2}$ , we compare them with the available results obtained within the finite- $T$  DMRG and Lanczos methods. We find an excellent agreement, as shown in Figs. 4(a) and 4(b).

The DMFT and HEOM results are crosschecked with the path integral QMC calculations. The quantity that we obtain in QMC is the single electron correlation function in imaginary time, which can be expressed through the spectral function as  $C_k(\tau) = \int_{-\infty}^{\infty} d\omega e^{-\omega\tau} A_k(\omega)$ . Typical results are illustrated in Figs. 4(c) and 4(d), while extensive comparisons are presented in Sec. IX of SM [46]. At  $T = 0.4$  we can see a small difference in  $C_\pi(\tau)$  between the DMFT and QMC (HEOM) results. At  $T = 1$ , both for  $k = 0$  and  $k = \pi$ , the difference in  $C_k(\tau)$  is minuscule, well below the QMC error bar, which is smaller than the symbol size. This confirms that nonlocal correlations are weak. Similarly, as for the spectral functions, the SCMA correlation functions show clear deviation from other solutions. We, however, note that great care is needed when drawing conclusions from the imaginary axis data since a very small difference in the imaginary axis correlation functions can correspond to substantial differences in spectral functions.

*Conclusions.*—In summary, we have presented a comprehensive solution of the 1D Holstein polaron covering all parameter regimes. We showed that the DMFT is a remarkably good approximation in the whole parameter space. This approximation is simple, numerically efficient, and can also be easily applied in two and three dimensions. We successfully used momentum-space HEOM and ED methods for comparisons with the DMFT spectral functions both at zero and at finite temperature. The comparisons showed an excellent agreement between the spectral functions in most of the parameter space. For parameters that are most challenging for the DMFT, a very good agreement was found around  $k = 0$  and a reasonably good agreement was obtained at larger values of  $k$ . All of the results are crosschecked with the imaginary axis QMC calculations and with the available results from the literature. Both the DMFT and HEOM methods are implemented directly in real frequency, without artificial broadening of the spectral functions. This will be crucial in order to calculate dynamical quantities and determine a potential role of the vertex corrections to conductivity by avoiding possible pitfalls of the analytical continuation, which we leave as a challenge for future work.

D. T. acknowledges useful discussions with V. Dobrosavljević. We thank J. Bonča for sharing with us the data from Ref. [23]. The authors acknowledge funding provided by the Institute of Physics Belgrade, through the grant by the Ministry of Education, Science, and Technological Development of the Republic of Serbia. Numerical simulations were performed on the PARADOX supercomputing facility at the Scientific Computing Laboratory, National Center of Excellence for the Study of Complex Systems, Institute of Physics Belgrade.

- 
- [1] T. Holstein, *Ann. Phys. (N.Y.)* **8**, 325 (1959).  
 [2] A. S. Alexandrov, *Polarons in Advanced Materials* (Springer, New York, 2007).  
 [3] C. Franchini, M. Reticcioli, M. Setvin, and U. Diebold, *Nat. Rev. Mater.* **6**, 560 (2021).  
 [4] L. Vidmar, J. Bonča, M. Mierzejewski, P. Prelovšek, and S. A. Trugman, *Phys. Rev. B* **83**, 134301 (2011).  
 [5] B. Kloss, D. R. Reichman, and R. Tempelaar, *Phys. Rev. Lett.* **123**, 126601 (2019).  
 [6] C. Brockt and E. Jeckelmann, *Phys. Rev. B* **95**, 064309 (2017).  
 [7] N. Prodanović and N. Vukmirović, *Phys. Rev. B* **99**, 104304 (2019).  
 [8] J. Stolpp, J. Herbrych, F. Dorfner, E. Dagotto, and F. Heidrich-Meisner, *Phys. Rev. B* **101**, 035134 (2020).  
 [9] Y. Murakami, P. Werner, N. Tsuji, and H. Aoki, *Phys. Rev. B* **91**, 045128 (2015).  
 [10] D. Jansen, J. Stolpp, L. Vidmar, and F. Heidrich-Meisner, *Phys. Rev. B* **99**, 155130 (2019).  
 [11] J. H. Fetherolf, D. Golež, and T. C. Berkelbach, *Phys. Rev. X* **10**, 021062 (2020).  
 [12] A. S. Mishchenko, N. Nagaosa, and N. Prokof'ev, *Phys. Rev. Lett.* **113**, 166402 (2014).  
 [13] M. Kang, S. W. Jung, W. J. Shin, Y. Sohn, S. H. Ryu, T. K. Kim, M. Hoesch, and K. S. Kim, *Nat. Mater.* **17**, 676 (2018).  
 [14] G. Mahan, *Many-Particle Physics* (Kluwer Academic, New York, 2000).  
 [15] I. Lang and Y. A. Firsov, *Zh. Eksp. Teor. Fiz.* **43**, 1843 (1962) [*Sov. Phys. JETP* **16**, 1301 (1963)].  
 [16] A. S. Alexandrov and J. T. Devreese, *Advances in Polaron Physics* (Springer, New York, 2010).  
 [17] E. Jeckelmann and S. R. White, *Phys. Rev. B* **57**, 6376 (1998).  
 [18] C. Zhang, E. Jeckelmann, and S. R. White, *Phys. Rev. B* **60**, 14092 (1999).  
 [19] P. E. Kornilovitch, *Phys. Rev. Lett.* **81**, 5382 (1998).  
 [20] A. H. Romero, D. W. Brown, and K. Lindenberg, *J. Chem. Phys.* **109**, 6540 (1998).  
 [21] A. H. Romero, D. W. Brown, and K. Lindenberg, *Phys. Rev. B* **59**, 13728 (1999).  
 [22] J. Bonča, S. A. Trugman, and I. Batistić, *Phys. Rev. B* **60**, 1633 (1999).  
 [23] J. Bonča, S. A. Trugman, and M. Berciu, *Phys. Rev. B* **100**, 094307 (2019).  
 [24] D. Jansen, J. Bonča, and F. Heidrich-Meisner, *Phys. Rev. B* **102**, 165155 (2020).  
 [25] Y. Tanimura, *J. Chem. Phys.* **153**, 020901 (2020).  
 [26] R.-X. Xu and Y. J. Yan, *Phys. Rev. E* **75**, 031107 (2007).  
 [27] J. Jin, X. Zheng, and Y. J. Yan, *J. Chem. Phys.* **128**, 234703 (2008).  
 [28] D. Hou, R. Wang, X. Zheng, N. H. Tong, J. H. Wei, and Y. J. Yan, *Phys. Rev. B* **90**, 045141 (2014).  
 [29] Z. H. Li, N. H. Tong, X. Zheng, D. Hou, J. H. Wei, J. Hu, and Y. J. Yan, *Phys. Rev. Lett.* **109**, 266403 (2012).  
 [30] L. Chen, Y. Zhao, and Y. Tanimura, *J. Phys. Chem. Lett.* **6**, 3110 (2015).  
 [31] L. Song and Q. Shi, *J. Chem. Phys.* **142**, 174103 (2015).  
 [32] L. Song and Q. Shi, *J. Chem. Phys.* **143**, 194106 (2015).  
 [33] I. S. Dunn, R. Tempelaar, and D. R. Reichman, *J. Chem. Phys.* **150**, 184109 (2019).  
 [34] Y. Yan, T. Xing, and Q. Shi, *J. Chem. Phys.* **153**, 204109 (2020).  
 [35] M. Hohenadler, M. Aichhorn, and W. von der Linden, *Phys. Rev. B* **68**, 184304 (2003).  
 [36] G. De Filippis, V. Cataudella, V. Marigliano Ramaglia, and C. A. Perroni, *Phys. Rev. B* **72**, 014307 (2005).  
 [37] M. Berciu, *Phys. Rev. Lett.* **97**, 036402 (2006).  
 [38] G. L. Goodvin, M. Berciu, and G. A. Sawatzky, *Phys. Rev. B* **74**, 245104 (2006).  
 [39] A. Georges, G. Kotliar, W. Krauth, and M. J. Rozenberg, *Rev. Mod. Phys.* **68**, 13 (1996).  
 [40] R. M. Martin, L. Reining, and D. M. Ceperley, *Interacting Electrons: Theory and Computational Approaches* (Cambridge University Press, Cambridge, England, 2016).  
 [41] S. Ciuchi, F. de Pasquale, S. Fratini, and D. Feinberg, *Phys. Rev. B* **56**, 4494 (1997).  
 [42] S. Fratini, F. de Pasquale, and S. Ciuchi, *Phys. Rev. B* **63**, 153101 (2001).  
 [43] S. Fratini and S. Ciuchi, *Phys. Rev. Lett.* **91**, 256403 (2003).  
 [44] L.-C. Ku, S. A. Trugman, and J. Bonča, *Phys. Rev. B* **65**, 174306 (2002).

- [45] V. Janković and N. Vukmirović, *Phys. Rev. B* **105**, 054311 (2022).
- [46] See Supplemental Material at <http://link.aps.org/supplemental/10.1103/PhysRevLett.129.096401> for detailed analysis and supporting data.
- [47] J. Vučičević, J. Kokalj, R. Žitko, N. Wentzell, D. Tanasković, and J. Mravlje, *Phys. Rev. Lett.* **123**, 036601 (2019).
- [48] A. Vranić, J. Vučičević, J. Kokalj, J. Skolimowski, R. Žitko, J. Mravlje, and D. Tanasković, *Phys. Rev. B* **102**, 115142 (2020).
- [49] A. Migdal, *Zh. Eksp. Teor. Fiz.* **34**, 1438 (1958) [*Sov. Phys. JETP* **7**, 996 (1958)].
- [50] H. De Raedt and A. Lagendijk, *Phys. Rev. Lett.* **49**, 1522 (1982).
- [51] H. De Raedt and A. Lagendijk, *Phys. Rev. B* **27**, 6097 (1983).
- [52] H. De Raedt and A. Lagendijk, *Phys. Rev. B* **30**, 1671 (1984).
- [53] O. S. Barišić, *Phys. Rev. B* **76**, 193106 (2007).